ACS APPLIED MATERIALS & INTERFACES

www.acsami.org

Research Article

Thickness-Dependent Cross-Plane Thermal Conductivity Measurements of Exfoliated Hexagonal Boron Nitride

Gabriel R. Jaffe,* Keenan J. Smith, Kenji Watanabe, Takashi Taniguchi, Max G. Lagally, Mark A. Eriksson, and Victor W. Brar

Cite This: *ACS Appl. Mater. Interfaces* 2023, 15, 12545−12550

Read Online

ACCESS | Metrics & More | Article Recommendations | Supporting Information

ABSTRACT: Submicrometer-thick layers of hexagonal boron nitride (hBN) exhibit high in-plane thermal conductivity and useful optical properties, and serve as dielectric encapsulation layers with low electrostatic inhomogeneity for graphene devices. Despite the promising applications of hBN as a heat spreader, the thickness dependence of its cross-plane thermal conductivity is not known, and the cross-plane phonon mean free paths (MFPs) have not been measured. We measure the cross-plane thermal conductivity of hBN flakes exfoliated from bulk crystals. We find that submicrometer thick flakes exhibit thermal conductivities up to 8.1 ± 0.5 W m^{-1} K^{-1} at 295 K, which exceeds previously reported bulk values by more than 60%. Surprisingly, the average phonon mean free path is found to be several hundred nanometers at room temperature, a factor of 5 larger than previous predictions. When planar twist interfaces are introduced into the crystal by mechanically stacking multiple thin flakes, the cross-plane thermal conductivity of the stack is found to be a factor of 7 below that of individual flakes with similar total thickness, thus providing strong evidence that phonon scattering at twist boundaries limits the maximum phonon MFPs. These results have important implications for hBN integration in nanoelectronics and improve our understanding of thermal transport in two-dimensional materials.

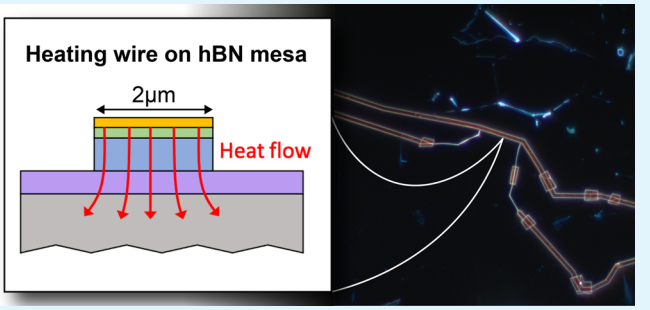

KEYWORDS: *phonon, mean free path, hBN, cross-plane, thermal conductivity, twist interface*

INTRODUCTION

Effectively dissipating heat away from hotpots caused by high-power or densely packed electronic structures is an outstanding thermal management problem. Heat-spreading films must exhibit high thermal conductivity and good dielectric characteristics, and form smooth clean interfaces with heat-emitting structures to reduce hotspot temperatures. Hexagonal boron nitride (hBN), a wide-bandgap dielectric two-dimensional (2D) material, has drawn significant research interest for its high in-plane thermal conductivity,[1−3] its use as a charge-trap free encapsulation material for graphene electronics,[4,5] and its optical characteristics.[6] Films of hBN can be mechanically cleaved from bulk crystals and transferred with atomically smooth and clean interfaces. Such transferred films have demonstrated significant heat-spreading capability in LED devices and graphene electronics.[7,8] The clean and conformal nature of these flexible hBN films has distinct advantages over materials such as diamond or SiC, which require thermally resistive interface layers to bond to other materials and suffer from growth defects near the interface layer.[9,10]

The rate at which a hotspot can be cooled is determined by the strength of the three-dimensional heat flow through a surrounding heat-spreading film. Many 2D materials have a high degree of anisotropy in their thermal conductivities. While they exhibit some of the highest known conductivities along their in-plane directions, they often have relatively small cross-plane thermal conductivities. The high in-plane thermal conductivities make these materials excellent candidates for heat-spreading in nanoelectronics,[11,12] and the anisotropic thermal transport properties have found applications in thermoelectrics and thermal isolation of temperature-sensitive components.[13−16] The thermal conductivities of most bulk 2D crystals are well-known; however, at submicrometer length scales, the thermal conductivity of 2D materials can exhibit a strong thickness dependence. Once the thickness of a film is less than the average phonon mean free path, the thermal conductivity begins to decrease. It is therefore necessary to know the mean free paths (MFPs) of the phonons responsible for heat transport to form an accurate model of thermal

Received: December 1, 2022
Accepted: February 13, 2023
Published: February 27, 2023

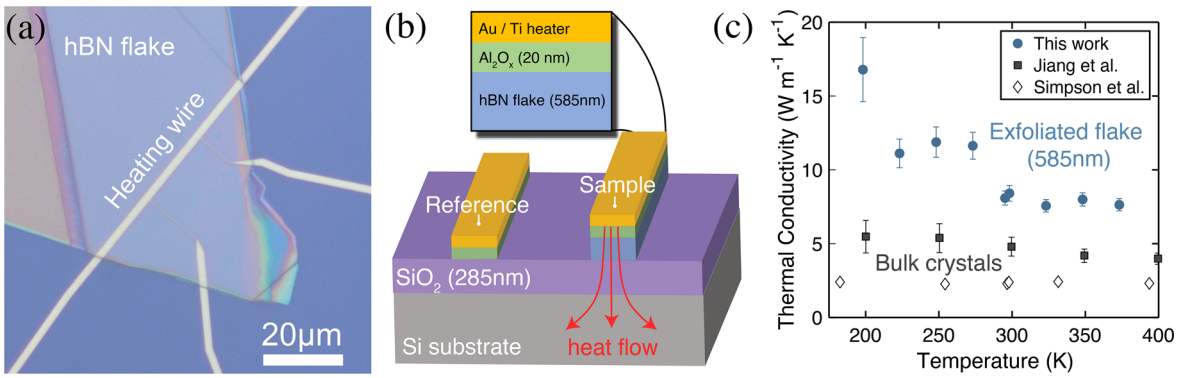

Figure 1. (a) An optical image of a four-probe heating wire fabricated across an AlO_x-encapsulated hBN flake that has been exfoliated from a bulk crystal and mechanically transferred to a SiO_2/Si substrate. (b) A cross-sectional schematic diagram of a reference heating wire on the AlO_x covered SiO_2 substrate and a second wire on a hBN sample. The encapsulating AlO_x layer and underlying hBN are etched into a mesa as shown using BCl_3Ar and SF_6 plasma etches, respectively. During a measurement, the heat from the wire flows cross-plane through the hBN and dissipates into the substrate. (c) The measured cross-plane thermal conductivity of a 585 nm thick hBN flake as a function of temperature. The cross-plane thermal conductivity of bulk hBN crystals (>10 μm thick) is shown as "■" and "◇" for comparison.[20,21]

conductivity in the submicrometer regime.[17] Recently, the phonon MFP spectra of graphite and MoS_2 were measured, and the phonon MFPs were found to be hundreds of nanometers at room temperature, far exceeding kinetic-theory estimates.[18,19] It is currently not known whether other two-dimensional materials also exhibit these long phonon MFPs and to what degree scattering mechanisms such as grain boundaries limit the maximum phonon MFPs.

For bulk hBN (>10 μm thick), the cross-plane thermal conductivity has been measured to be ~2−5 W m^{-1} K^{-1},[3,20,21] and the average cross-plane phonon MFP has been predicted from first-principles calculations to be ~18 nm at 300 K.[21] This prediction is an order of magnitude lower than the average MFPs measured in graphite and MoS_2 and has not been verified experimentally. An empirical estimate of the average cross-plane phonon mean free path, Λ_{avg}, can be calculated from kinetic theory using $\kappa_{bulk} = (1/3)Cv_g\Lambda_{avg}$, where κ_{bulk} is the bulk cross-plane thermal conductivity, C is the heat capacity, and v_g is the average group velocity of the cross-plane acoustic phonon modes. When we use κ = 2−5 W m^{-1} K^{-1}, C = 1.8 J cm^{-3} K^{-1},[20] and v_g = 3800 m s^{-1},[21] this results in an average MFP estimate of 0.9−2.2 nm, an order of magnitude below predictions.

In this Article, we report cross-plane thermal-conductivity measurements of submicrometer-thick exfoliated hBN flakes as a function of thickness and temperature. The cross-plane thermal conductivity of a 585 nm thick flake is measured to be 60% larger than the highest conductivity of bulk hBN reported in the literature. The thin flakes and high-quality samples enable measurements of the physics governing short and long-mean-free-path phonons. We find that the flake thermal conductivity exhibits a strong thickness dependence, decreasing by a factor of 40 from 8.1 ± 0.5 W m^{-1} K^{-1} for a 585 nm thick flake to 0.20 ± 0.06 W m^{-1} K^{-1} for a 7 nm thick flake. Fits to the data indicate that the majority of the heat is carried by phonons with mean free paths >100 nm. This value far exceeds the MFPs estimated from kinetic theory, which predicts MFPs of only a few nanometers, as well as the prediction from first-principles calculations that ~80% of the heat is carried by phonons with MFPs between 3−90 nm.[3] We further demonstrate that stacking faults can drastically reduce the cross-plane thermal conductivity of hBN by mechanically stacking five ~15 nm exfoliated flakes. The stacked structure is found to have a cross-plane thermal conductivity a factor of 7 below that of individual flakes with the same total thickness as the stack. This result suggests that variations in the densities of stacking faults in bulk samples could explain the differences in reported hBN bulk thermal conductivities and the high conductivity reported here.

Taken together, the long MFPs and strong interface scattering we report have two important implications. First, the long phonon MFPs in hBN impact its use in heat-spreading applications in nanoelectronics, because the cross-plane thermal conductivity of hBN will decrease dramatically as the film thickness is reduced below the phonon MFPs. Heat dissipation from hotspots in electronics flows both in-plane and cross-plane through a heat-spreading film. It is often desirable to make heat-spreading films as thin as possible so as to maximize their cross-plane thermal conductance. Our results demonstrate that the cross-plane thermal conductance of hBN does not significantly increase for films <300 nm thick. Second, these results demonstrate that two-dimensional materials are a promising model system for studying coherent phonon transport behavior, because heterostructures of dissimilar materials with layer thicknesses far below the typical phonon MFPs can be fabricated with smooth and pristine interfaces by stacking different exfoliated flakes at arbitrary angles.

The thermal conductivity of hBN, κ (units of W m^{-1} K^{-1}), as a function of thickness, d, can be expressed as

$$\kappa(d) = \frac{d}{R_{therm}(d) \times A} \quad (1)$$

where $R_{therm}(d)$ (units of m^2 K GW^{-1}) is the total cross-plane thermal resistance and A is the surface area of a hBN flake of thickness d. We measure $R_{therm}(d)$ using a differential three-omega measurement where the temperature of a reference heating wire on the bare sample substrate is subtracted from the temperature rise of a heating wire on an hBN flake, as seen in Figure 1b.[22−27] This temperature difference can be converted to a measure of thermal resistance, R_{therm}, from which the thermal conductivity can be calculated using eq 1. For this technique, a metal four-probe wire is fabricated across the film of interest and is then used as both a heater and a thermometer. Figure 1a shows an optical image of a heating wire on an hBN flake. The heating wires are 2 μm wide, the distance between the voltage probes is 20 μm, and the voltage

https://doi.org/10.1021/acsami.2c21306
ACS Appl. Mater. Interfaces 2023, 15, 12545−12550

probe widths are 300 nm where they make contact with the heating wire. Bond pads are fabricated >400 μm away from the section of wire between the voltage probes to prevent heat dissipating out through the wire bonds from affecting the experiment.

The hBN flakes are exfoliated in a glovebox with nitrogen atmosphere and transferred onto SiO_2/Si substrates. The flakes are vacuum annealed under an Ar/H_2 flow at 350 °C for 1 h. An atomic force microscope is used to measure the flake thicknesses and surface roughnesses. The flakes are encapsulated in a 20 nm thick layer of AlO_x deposited by atomic-layer deposition to protect the interface between the flake and substrate from solvent contamination during processing. Metal four-probe heater/thermometer wires are fabricated on the sample surface using electron-beam lithography. The Au wires are 65 nm thick with a 5 nm Ti adhesion layer. Small metal interconnects are patterned on the edges of flakes with thicknesses >60 nm to connect the wires over the large jumps in the surface topography. To ensure that the heat flowing out of the wire through the hBN flakes is entirely cross-plane, the hBN flakes are etched into mesas, as shown in Figure 1b, using first a BCl_3Ar plasma etch to remove the AlO_x layer, and then a SF_6 plasma etch to remove the hBN.

RESULTS AND DISCUSSION

Figure 1c shows a comparison of the cross-plane thermal conductivity as a function of temperature of the thickest flake measured here (585 nm) to that of bulk hBN samples (>10 μm thick) by others.[20,21] The thick flake exhibits a larger thermal conductivity than previous bulk measurements across the entire temperature range of ∼200−400 K. Additionally, the thermal conductivity increases by a factor of ∼2 between room temperature and 200 K, similar to that of other materials known to have large phonon mean free paths, such as Si.[28] The temperature dependence of hBN reported here is more pronounced than previous studies of graphite where phonon scattering at stacking faults limited the thermal conductivity at low temperatures.[18] In Figure 2a we report the measured cross-plane thermal resistance of the hBN flakes as a function of flake thickness at 295 K, and the calculated thermal conductivity using eq 1 is shown in Figure 2b. Additional temperature-dependent thermal conductivity data can be found in the Supporting Information.

We observe that the thermal conductivity more than doubles as the flake thickness increases from 200 to 585 nm, indicating that phonons with MFPs of several hundred nanometers make significant contributions to the thermal conductivity of the thicker flakes. Moreover, the thermal conductivity appears to be gradually saturating with increasing thickness, consistent with similar trends seen in graphite.[18] For the thickest flakes that we measure, the thermal conductivities exceed previously measured bulk values, which are shown in Figure 2b as shaded orange, green, and red squares.[3,20,21] We note that the thermal conductivity of hBN is known to vary significantly with crystal defect density and that hBN samples with the lowest previously measured cross-plane thermal conductivity (∼2 W m^{-1} K^{-1}) were found to have an average crystallite size in the cross-plane direction of ∼10 nm.[20] The hBN crystals studied in this work are expected to have millimeter-scale grain sizes.[4,29] In Figure 1a we observe flat regions of uniform thickness >50 μm across.

For an infinitely thick film, the differential mean free path contribution function $f(\Lambda)$ describes the fractional contribution of phonons with mean free path Λ to the thermal

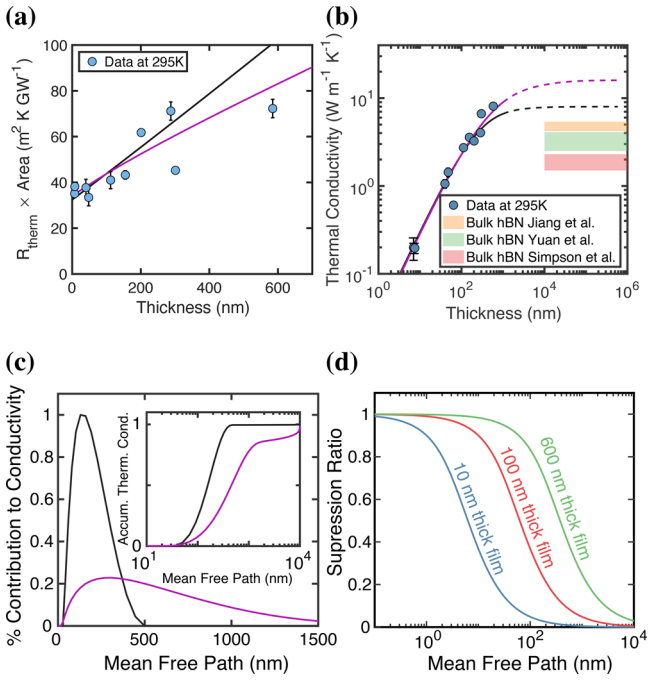

Figure 2. (a) The measured cross-plane thermal resistance of the hBN flakes multiplied by the surface area of the heating wire as a function of flake thickness at 295 K (blue points). The phonon mean free path contribution fits to the data assuming that the thermal conductivity eventually saturates to either 8 or 16 W m^{-1} K^{-1} are shown as black and purple lines, respectively. (b) The hBN flake cross-plane thermal conductivity at 295 K (blue points) calculated from the data shown in (a). Shaded regions indicate the thermal conductivity of bulk (>10 μm) hBN measured by others.[3,20,21] The black and purple lines show the phonon mean free path contribution fits. The dashed lines indicate the likely trend in the thermal conductivity when extrapolated to larger thicknesses. (c) The differential phonon mean free path functions that best fit the data shown in (a) assuming two different values for the bulk thermal conductivity κ_{bulk}. The inset shows the corresponding thermal conductivity accumulation functions. (d) The suppression of contributions to thermal conductivity (eq 2) of phonons with long mean free paths for films of three different thicknesses.

conductivity.[30] The contributions from phonons with long mean free paths are suppressed in a film of finite thickness. The suppression of phonon contributions to thermal conductivity for the sample geometry considered here is described by the suppression function:

$$S(K_n) = 1 - K_n(1 - e^{-1/K_n}) \quad (2)$$

where the Knudsen number K_n is defined as $K_n = \Lambda/L$ and L is the film thickness.[18] The thermal conductivity of a thin film as a function of film thickness $\kappa(L)$ is a convolution of $f(\Lambda)$ and $S(K_n)$ over all phonon mean free paths:

$$\kappa(L) = \int_0^\infty S(K_n) f(\Lambda)\, d\Lambda \quad (3)$$

We find the differential mean free path contribution functions that best fit our thermal conductivity data at 295 K using a convex optimization procedure and a Gaussian quadrature discretization of the integral in eq 3.[30] Additional information about the fitting procedure is available in the Supporting Information. Although the thermal conductivity appears to be rolling off at large thicknesses in Figure 2b, we do not know the saturation thickness for hBN or the bulk thermal

https://doi.org/10.1021/acsami.2c21306
ACS Appl. Mater. Interfaces 2023, 15, 12545−12550

conductivity of an infinitely thick flake. We therefore provide, in Figure 2b, the mean-free-path fits to the data assuming a bulk conductivity of either 8 or 16 W m^{-1} K^{-1}, which both can provide good fits to our measurements depending on the assumed phonon MFP distribution. The accompanying best-fit phonon mean-free-path contribution functions are shown in Figure 2c. In both fits, we find that phonons with mean free paths >100 nm are responsible for the majority of the thermal transport. The thermal conductivities as a function of thickness calculated from the fits are shown as lines in Figure 2b. We find that all of the fits are in close agreement for thicknesses <200 nm and begin to diverge at larger thicknesses.

The measured thermal resistance of the hBN likely includes some small contributions from the interfacial thermal resistances (ITRs) between the hBN and surrounding materials.[18,19] The thermal conductivity reported in Figure 2 therefore represents a conservative lower bound. We account for possible ITR contributions by expressing the measured total thermal resistance, $R_{\text{therm}}(d)$, as

$$R_{\text{therm}}(d) = R_{\text{hBN}}(d) + R_{\text{ITR}} \tag{4}$$

where $R_{\text{hBN}}(d)$ is the thermal-resistance contribution of phonon scattering within the hBN layer and R_{ITR} is the interfacial-thermal-resistance contribution given by

$$R_{\text{ITR}} = \text{ITR}_{(\text{Al}_2\text{O}_x/\text{hBN})} + \text{ITR}_{(\text{hBN}/\text{SiO}_2)} - \text{ITR}_{(\text{Al}_2\text{O}_x/\text{SiO}_2)} \tag{5}$$

Here, $\text{ITR}_{(\text{Al}_2\text{O}_x/\text{hBN})}$ and $\text{ITR}_{(\text{hBN}/\text{SiO}_2)}$ are the interfacial thermal resistances on the top and bottom surfaces of the hBN flake, respectively, and $\text{ITR}_{(\text{Al}_2\text{O}_x/\text{SiO}_2)}$ is the interfacial thermal resistance between the two oxide layers under the reference heater. To our knowledge, there are no published measurements of these interfacial thermal resistances. Furthermore, the ITRs are dependent on the microscopic conditions of the interface and will vary from sample to sample.

While we cannot directly measure these interface resistances, we can leverage the fact that interfacial thermal resistances do not vary significantly with temperature,[31] whereas the thermal resistance of the hBN decreases with temperature.[21] We set an upper bound on the interface resistances in our data by assuming that at low temperatures the hBN thermal resistance is negligible, $R_{\text{hBN}} = 0$, and therefore all thermal resistance we measure arises purely from interface scattering. The lowest-temperature data we report are at 198 K, seen in Figure 3a as red points. The measured thermal resistance at 198 K is subtracted from the resistance measured at 295 K, which produces the trend show in Figure 3b (orange points). In Figure 3c we show the thermal conductivities as a function of thickness calculated using eq 1 (orange points) and fit the data with differential mean-free-path contribution functions, assuming the bulk conductivity is either 8, 16, or 32 W m^{-1} K^{-2} (solid lines). The conductivities calculated without considering the ITRs are shown as blue points for comparison. It is clear that removing the ITR contribution increases the calculated thermal conductivity and that the data are now only well described by the fits using the higher bulk thermal conductivities of 16 or 32 W m^{-1} K^{-2} (purple and blue lines). The average phonon mean free paths from these fits are 87 and 343 nm, respectively. In summary, this interface analysis raises the expected bulk thermal conductivity of hBN and does not significantly reduce the extracted phonon mean free paths.

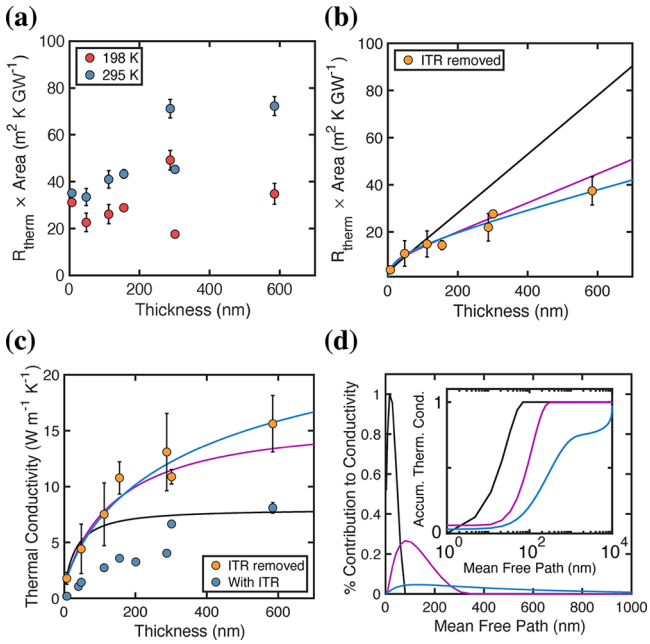

Figure 3. (a) The measured cross-plane thermal resistance of the hBN flakes multiplied by the surface area of the heating wire as a function of flake thickness at 295 K (blue points) and 198 K (red points). (b) The cross-plane thermal resistance at 198 K is subtracted from the resistance at 295 K to remove the interfacial thermal resistance contribution (ITR). The remaining thermal resistance (orange points) is due solely to heat conduction in the hBN flake. The phonon mean free path contribution fits to the data assuming that the thermal conductivity eventually saturates to either 8, 16, or 32 W m^{-1} K^{-1} are shown as black, purple, and blue lines, respectively. (c) The calculated thermal conductivity of hBN with the ITR contribution removed (orange points) and without the subtraction (blue points). The thermal conductivity fits to the ITR removed data points are shown as solid lines. (d) The differential phonon mean free path spectra that best fit the orange data points shown in (b) assuming three different values for the bulk thermal conductivity κ_{bulk}. The inset shows the corresponding thermal conductivity accumulation functions.

Phonon grain boundary scattering at stacking faults (planar twist interfaces) has been proposed as a limiting factor for the maximum possible phonon MFPs in two-dimensional materials. Studies of graphite correlated the maximum observed phonon MFPs with the average spacing between twist grain boundaries found in cross-sectional TEM images.[18] This hypothesis is further supported by studies of WSe_2 crystals grown with random rotational mismatches between each successive layer that found that twist interfaces reduced the cross-plane thermal conductivity by a factor of 30 below that of single-crystal samples.[32] Molecular-dynamics simulations of twist interfaces of both graphite and hBN have also shown that such grain boundaries can significantly reduce the cross-plane thermal conductivity.[33]

To investigate the effects of grain boundary scattering in hBN, we introduce twist interfaces into a hBN crystal by mechanically stacking five exfoliated hBN flakes. The total stack thickness is measured with an atomic force microscope to be 74 ± 2 nm, and the individual layer thicknesses are estimated using optical contrast to be (from bottom to top) 26, 19, 11, 10, and 8 nm, respectively. Figure 4a shows a schematic diagram of the stacked flakes, and Figure 4b shows an optical image of the heating wire fabricated over the stack before the

https://doi.org/10.1021/acsami.2c21306
ACS Appl. Mater. Interfaces 2023, 15, 12545−12550

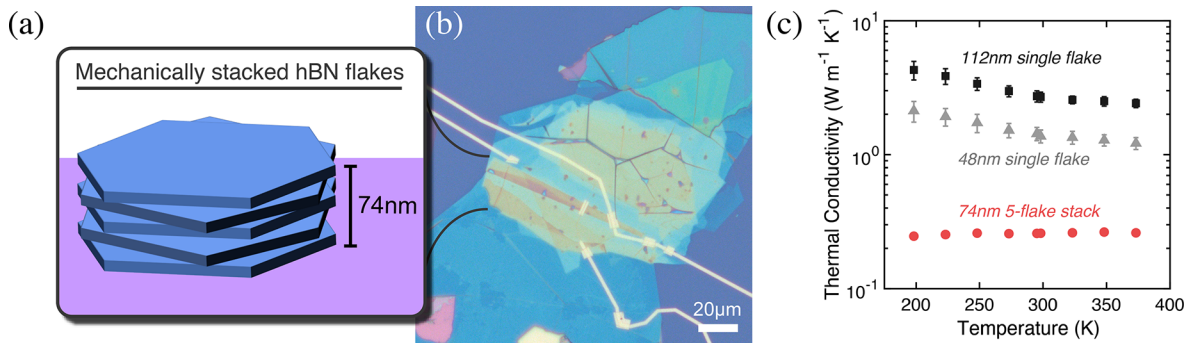

Figure 4. (a) A schematic diagram showing a heterostructure consisting of five exfoliated hBN flakes mechanically stacked with arbitrary rotational mismatches between each flake. (b) An optical image of the heating wire fabricated across the five-flake stack. (c) The measured cross-plane thermal conductivity as a function of temperature of the five-flake stack shown in (b), which had a total thickness of 74 nm, is shown in red. The "■" and gray "▲" are the thermal conductivities of individual flakes from Figure 2 with thicknesses of 112 and 48 nm, respectively.

hBN is etched into a mesa. The residue present between flakes in such stacked structures has been found to clump up into large bubbles after annealing.[34] The heating wires are specifically designed on each sample to route around the bubbles to provide a measurement of only the atomically clean interface regions. Dark-field optical imaging is used to identify regions without bubbles or residue, an example image of which can be found in the Supporting Information.

We measure the cross-plane thermal conductivity of the five-flake stack and compare the results to the thermal conductivity of individual flakes of similar thicknesses as a function of temperature in Figure 4c. We calculate the expected thermal conductivity of a 74 nm flake to be 2.00 W m^{-1} K^{-1} at 295 K by averaging the values from the fits at that thickness in Figure 2b. By comparison, we measure the thermal conductivity of the five-flake stack to be 0.26 ± 0.01 W m^{-1} K^{-1}, more than a factor of 7 below this estimate and equivalent to that of a single ∼9 nm flake. This indicates that strong phonon scattering at the twist interfaces has drastically reduced the phonon MFPs, thereby reducing the thermal conductivity. Furthermore, the thermal conductivity of the stack does not increase at lower temperatures, suggesting that the thermal conductivity is dominated by interface scattering.

CONCLUSION

Our results show that the cross-plane thermal conductivity of hBN is higher than previously thought. We measure it to be 8.1 ± 0.5 W m^{-1} K^{-1}, but when interfaces are considered, it can be as large as 15.6 ± 2.5 W m^{-1} K^{-1}. Our low-defect-density samples allow us to measure the thickness dependence of the thermal conductivity, thereby providing access to the phonon mean free paths, which we find to be hundreds of nanometers in length, far exceeding previous predictions. We demonstrate that the thermal conductivity of thicker films of hBN can be significantly reduced by stacking multiple thin flakes of hBN with arbitrary rotational mismatches between each layer. The ability to stack hBN flakes at controlled angles and potentially incorporate layers of other two-dimensional materials with long phonon MFPs, such as graphite and MoS_2, presents interesting opportunities to explore phonon interface scattering as parameters such as twist angle, layer thickness, and phonon mode mismatch between layers are varied. The data presented here have important implications for thermal-management efforts to incorporate hBN as a heat-spreading material, providing the necessary information for determining how the cross-plane thermal conductivity of hBN films will scale with film thickness.

ASSOCIATED CONTENT

Supporting Information

The Supporting Information is available free of charge at https://pubs.acs.org/doi/10.1021/acsami.2c21306.

Phonon mean free path fitting procedure, temperature-dependent thermal conductivity data for multiple flake thicknesses, and device optical characterization (PDF)

AUTHOR INFORMATION

Corresponding Author

Gabriel R. Jaffe − *Department of Physics, University of Wisconsin-Madison, Madison, Wisconsin 53706, United States;* orcid.org/0000-0003-2672-0375; Email: gjaffe@wisc.edu

Authors

Keenan J. Smith − *Department of Physics, University of Wisconsin-Madison, Madison, Wisconsin 53706, United States*

Kenji Watanabe − *Research Center for Functional Materials, National Institute for Materials Science, Tsukuba 305-0044, Japan;* orcid.org/0000-0003-3701-8119

Takashi Taniguchi − *International Center for Materials Nanoarchitectonics, National Institute for Materials Science, Tsukuba 305-0044, Japan;* orcid.org/0000-0002-1467-3105

Max G. Lagally − *Department of Materials Science and Engineering, University of Wisconsin-Madison, Madison, Wisconsin 53706, United States*

Mark A. Eriksson − *Department of Physics, University of Wisconsin-Madison, Madison, Wisconsin 53706, United States*

Victor W. Brar − *Department of Physics, University of Wisconsin-Madison, Madison, Wisconsin 53706, United States*

Complete contact information is available at: https://pubs.acs.org/10.1021/acsami.2c21306

Notes

The authors declare no competing financial interest.

■ ACKNOWLEDGMENTS

Thermal transport measurements and theoretical modeling were performed with support from US DOE Basic Energy Sciences DE-FG02-03ER46028. hBN crystal exfoliation and stacking was performed with support from US DOE Basic Energy Sciences under award #DE-SC0020313. We acknowledge the use of facilities supported by NSF through the UW-Madison MRSEC (DMR-1720415) and electron beam lithography supported by the NSF MRI program (DMR-1625348). K.W. and T.T. acknowledge support from JSPS KAKENHI (Grant numbers 19H05790, 20H00354, and 21H05233). We thank Dr. Donald Savage for his helpful comments and suggestions.

■ REFERENCES

(1) Sichel, E. K.; Miller, R. E.; Abrahams, M. S.; Buiocchi, C. J. Heat Capacity and Thermal Conductivity of Hexagonal Pyrolytic Boron Nitride. *Phys. Rev. B* **1976**, *13*, 4607−4611.
(2) Jo, I.; Pettes, M. T.; Kim, J.; Watanabe, K.; Taniguchi, T.; Yao, Z.; Shi, L. Thermal Conductivity and Phonon Transport in Suspended Few-Layer Hexagonal Boron Nitride. *Nano Lett.* **2013**, *13*, 550−554.
(3) Yuan, C.; Li, J.; Lindsay, L.; Cherns, D.; Pomeroy, J. W.; Liu, S.; Edgar, J. H.; Kuball, M. Modulating the Thermal Conductivity in Hexagonal Boron Nitride via Controlled Boron Isotope Concentration. *Communications Physics* **2019**, *2*, 43.
(4) Dean, C. R.; Young, A. F.; Meric, I.; Lee, C.; Wang, L.; Sorgenfrei, S.; Watanabe, K.; Taniguchi, T.; Kim, P.; Shepard, K. L.; Hone, J. Boron Nitride Substrates for High-Quality Graphene Electronics. *Nat. Nanotechnol.* **2010**, *5*, 722−726.
(5) Calado, V. E.; Goswami, S.; Nanda, G.; Diez, M.; Akhmerov, A. R.; Watanabe, K.; Taniguchi, T.; Klapwijk, T. M.; Vandersypen, L. M. K. Ballistic Josephson Junctions in Edge-Contacted Graphene. *Nat. Nanotechnol.* **2015**, *10*, 761−765.
(6) Cassbois, G.; Valvin, P.; Gil, B. Hexagonal Boron Nitride is an Indirect Bandgap Semiconductor. *Nat. Photonics* **2016**, *10*, 262−267.
(7) Choi, D.; Poudel, N.; Park, S.; Akinwande, D.; Cronin, S. B.; Watanabe, K.; Taniguchi, T.; Yao, Z.; Shi, L. Large Reduction of Hot Spot Temperature in Graphene Electronic Devices with Heat-Spreading Hexagonal Boron Nitride. *ACS Appl. Mater. Interfaces* **2018**, *10*, 11101−11107.
(8) Choi, I.; Lee, K.; Lee, C.-R.; Lee, J. S.; Kim, S. M.; Jeong, K.-U.; Kim, J. S. Application of Hexagonal Boron Nitride to a Heat-Transfer Medium of an InGaN/GaN Quantum-Well Green LED. *ACS Appl. Mater. Interfaces* **2019**, *11*, 18876−18884.
(9) Won, Y.; Cho, J.; Agonafer, D.; Asheghi, M.; Goodson, K. E. Fundamental Cooling Limits for High Power Density Gallium Nitride Electronics. *IEEE Transactions on Components, Packaging and Manufacturing Technology* **2015**, *5*, 737−744.
(10) Gu, Y.; Zhang, Y.; Hua, B.; Ni, X.; Fan, Q.; Gu, X. Interface Engineering Enabling Next Generation GaN-on-Diamond Power Devices. *J. Electron. Mater.* **2021**, *50*, 4239−4249.
(11) Yan, Z.; Liu, G.; Khan, J. M.; Balandin, A. A. Graphene Quilts for Thermal Management of High-Power GaN Transistors. *Nat. Commun.* **2012**, *3*, 827.
(12) Fu, Y.; Hansson, J.; Liu, Y.; Chen, S.; Zehri, A.; Samani, M. K.; Wang, N.; Ni, Y.; Zhang, Y.; Zhang, Z.-B.; Wang, Q.; Li, M.; Lu, H.; Sledzinska, M.; Torres, C. M. S.; Volz, S.; Balandin, A. A.; Xu, X.; Liu, J. Graphene Related Materials for Thermal Management. *2D Mater.* **2020**, *7*, 012001.
(13) Chen, C.-C.; Li, Z.; Shi, L.; Cronin, S. B. Thermoelectric Transport Across Graphene/Hexagonal Boron Nitride/Graphene Heterostructures. *Nano Res.* **2015**, *8*, 666−672.
(14) Kim, J. C.; Ren, Z.; Yuksel, A.; Dede, E. M.; Bandaru, P. R.; Oh, D.; Lee, J. Recent Advances in Thermal Metamaterials and Their Future Applications for Electronics Packaging. *J. Electron. Packaging* **2021**, *143*, 010801.
(15) Jeon, D.; Lim, J.; Bae, J.; Kadirov, A.; Choi, Y.; Lee, S. Suppression of Self-Heating in Nanoscale Interfaces using h-BN Based Anisotropic Heat Diffuser. *Appl. Surf. Sci.* **2021**, *543*, 148801.
(16) Li, Y.; Li, W.; Han, T.; Zheng, X.; Li, J.; Li, B.; Fan, S.; Qiu, C.-W. Transforming Heat Transfer with Thermal Metamaterials and Devices. *Nat. Rev. Mater.* **2021**, *6*, 488−507.
(17) Chen, G. Nonlocal and Nonequilibrium Heat Conduction in the Vicinity of Nanoparticles. *J. Heat Transfer* **1996**, *118*, 539−545.
(18) Zhang, H.; Chen, X.; Jho, Y.-D.; Minnich, A. J. Temperature-Dependent Mean Free Path Spectra of Thermal Phonons Along the c-Axis of Graphite. *Nano Lett.* **2016**, *16*, 1643−1649.
(19) Sood, A.; Xiong, F.; Chen, S.; Cheaito, R.; Lian, F.; Asheghi, M.; Cui, Y.; Donadio, D.; Goodson, K. E.; Pop, E. Quasi-Ballistic Thermal Transport Across MoS2 Thin Films. *Nano Lett.* **2019**, *19*, 2434−2442.
(20) Simpson, A.; Stuckes, A. D. The Thermal Conductivity of Highly Oriented Pyrolytic Boron Nitride. *J. Phys. C* **1971**, *4*, 1710−1718.
(21) Jiang, P.; Qian, X.; Yang, R.; Lindsay, L. Anisotropic Thermal Transport in Bulk Hexagonal Boron Nitride. *Phys. Rev. Mater.* **2018**, *2*, 064005.
(22) Cahill, D. G. Thermal Conductivity Measurement from 30 to 750 K: The 3w Method. *Rev. Sci. Instrum.* **1990**, *61*, 802−808.
(23) Cahill, D. G.; Katiyar, M.; Abelson, J. R. Thermal Conductivity of a-Si:H Thin Films. *Phys. Rev. B* **1994**, *50*, 6077−6081.
(24) Borca-Tasciuc, T.; Liu, W.; Liu, J.; Zeng, T.; Song, D. W.; Moore, C. D.; Chen, G.; Wang, K. L.; Goorsky, M. S.; Radetic, T.; Gronsky, R.; Koga, T.; Dresselhaus, M. S. Thermal Conductivity of Symmetrically Strained Si/Ge Superlattices. *Superlattices Microsctruct* **2000**, *28*, 199−206.
(25) Koh, Y. K.; Singer, S. L.; Kim, W.; Zide, J. M. O.; Lu, H.; Cahill, D. G.; Majumdar, A.; Gossard, A. C. Comparison of the 3 Omega Method and Time-Domain Thermoreflectance for Measurements of the Cross-Plane Thermal Conductivity of Epitaxial Semiconductors. *J. Appl. Phys.* **2009**, *105*, 054303.
(26) Jaffe, G. R.; Mei, S.; Boyle, C.; Kirch, J. D.; Savage, D. E.; Botez, D.; Mawst, L. J.; Knezevic, I.; Lagally, M. G.; Eriksson, M. A. Measurements of the Thermal Resistivity of InAlAs, InGaAs, and InAlAs/InGaAs Superlattices. *ACS Appl. Mater. Interfaces* **2019**, *11*, 11970−11975.
(27) Jaffe, G. R.; Smith, K. J.; Brar, V. W.; Lagally, M. G.; Eriksson, M. A. Three-Omega Thermal-Conductivity Measurements with Curved Heater Geometries. *Appl. Phys. Lett.* **2020**, *117*, 073102.
(28) Glassbrenner, C. J.; Slack, G. A. Thermal Conductivity of Silicon and Germanium from 3 K to the Melting Point. *Phys. Rev.* **1964**, *134*, A1058−A1069.
(29) Taniguchi, T.; Watanabe, K. Synthesis of High-Purity Boron Nitride Single Crystals Under High Pressure by Using Ba−BN Solvent. *J. Cryst. Growth* **2007**, *303*, 525−529.
(30) Minnich, A. J. Determining Phonon Mean Free Paths from Observations of Quasiballistic Thermal Transport. *Phys. Rev. Lett.* **2012**, *109*, 205901.
(31) Chen, Z.; Jang, W.; Bao, W.; Lau, C. N.; Dames, C. Thermal Contact Resistance Between Graphene and Silicon Dioxide. *Appl. Phys. Lett.* **2009**, *95*, 1−4.
(32) Chiritescu, C.; Cahill, D. G.; Nguyen, N.; Johnson, D.; Bodapati, A.; Keblinski, P.; Zschack, P. Ultralow Thermal Conductivity in Disordered, Layered WSe2 Crystals. *Science* **2007**, *315*, 351−353.
(33) Ouyang, W.; Qin, H.; Urbakh, M.; Hod, O. Controllable Thermal Conductivity in Twisted Homogeneous Interfaces of Graphene and Hexagonal Boron Nitride. *Nano Lett.* **2020**, *20*, 7513−7518.
(34) Haigh, S. J.; Gholinia, A.; Jalil, R.; Romani, S.; Britnell, L.; Elias, D. C.; Novoselov, K. S.; Ponomarenko, L. A.; Geim, A. K.; Gorbachev, R. Cross-Sectional Imaging of Individual Layers and Buried Interfaces of Graphene-Based Heterostructures and Superlattices. *Nat. Mater.* **2012**, *11*, 764−767.

https://doi.org/10.1021/acsami.2c21306
ACS Appl. Mater. Interfaces 2023, 15, 12545−12550